analytical chemistry

pubs.acs.org/ac Article

Detection of SARS-CoV-2 and Its Mutated Variants via CRISPR-Cas13-Based Transcription Amplification

Yuxi Wang,[#] Yong Zhang,[#] Junbo Chen, Minjin Wang, Ting Zhang, Wenxin Luo, Yalun Li, Yangping Wu, Bo Zeng, Kaixiang Zhang, Ruijie Deng,* and Weimin Li*

Cite This: https://dx.doi.org/10.1021/acs.analchem.0c04303 Read Online

ACCESS | Metrics & More | Article Recommendations | Supporting Information

ABSTRACT: The outbreak of severe acute respiratory syndrome coronavirus 2 (SARS-CoV-2) caused a global health emergency, and its gene mutation and evolution further posed uncertainty of epidemic risk. Herein, we reported a light-up CRISPR-Cas13 transcription amplification method, which enables the detection of SARS-CoV-2 and its mutated variants. Sequence specificity was ensured by both the ligation process and Cas13a/crRNA recognition, allowing us to identify viral RNA mutation. Light-up RNA aptamer allows sensitive output of amplification signals via target-activated ribonuclease activity of CRISPR-Cas13a. The RNA virus assay has been designed to detect coronavirus, SARS-CoV-2, Middle East respiratory syndrome (MERS), and SARS, as well as the influenza viruses such as, H1N1, H7N9, and H9N2. It was accommodated to sense as low as 82 copies of SARS-CoV-2. Particularly, it allowed us to strictly discriminate key mutation of the SARS-CoV-2 variant, D614G, which may induce higher epidemic and pathogenetic risk. The proposed RNA virus assays are promising for point-of-care monitoring of SARS-CoV-2 and its risking variants.

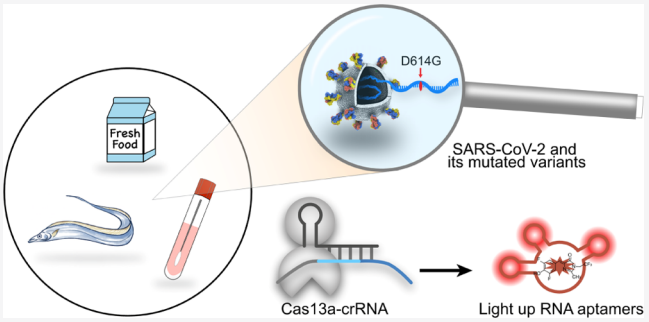

The worldwide outbreak of severe acute respiratory syndrome coronavirus 2 (SARS-CoV-2) has led us to a global health emergency. Until Oct 5th, 2020, coronavirus disease in 2019 (Covid-19) was reported to have infected 35.1 million people and caused more than 1 million deaths. Uniquely, RNA viruses exhibit high gene evolution rates because of the frequent error-prone replication.[1] The missense mutation, D614G, in the spike protein of SARS-CoV-2 has been reported to endow the SARS-CoV-2 virus with 10-fold higher infectivity, and it is now emerging as a predominant clade in some regions such as Europe.[2] Nevertheless, tools to rapidly resolve mutations in SARS-CoV-2 variants are still lacking. Timely diagnostic tests for RNA viruses and their key mutations will provide key data streams to inform strategies to mitigate pandemic outbreaks.

Nucleic acid (NA)-based tests directly target signature regions of RNA viruses and could, in principle, provide high accuracy and sensitivity for molecular diagnosis.[3−5] Thus, NA-based detection has become the gold standard for diagnosing RNA virus associated diseases, such as Covid-19 and Ebola.[6,7] In the Covid-19 pandemic outbreak, NA tests are intensively proceeded and play key roles in patient diagnosis and pandemic control.[4,6] In a typical NA test, target viral RNAs are transferred to cDNA via the reverse-transcription process, followed by either PCR or isothermal amplification to obtain abundant copies of target sequences.[8,9] PCR coupling with real-time fluorescence monitoring allows accurate and sensitive quantification of RNA viruses. Complementarily, isothermal amplification techniques such as recombinase polymerase amplification[10] and loop-mediated isothermal amplification (LAMP)[11,12] allow us to use precise temperature-control PCR instruments, facilitating NA tests in field laboratories and other resource-limited settings. Particularly, the introduction of CRISPR-based approaches using either Cas13a[13] or Cas12a[14] to detect amplified products further improves the sensitivity and sequence specificity of NA tests.[15−18] Albeit NA tests being a great success, the currently available NA-based test techniques have not been fully explored to profile the mutation of SARS-CoV-2, which can provide key information on infectivity and virulence. In addition, to specifically identify amplification products and record the amplification process, RNA/DNA probes are chemically modified with multiple tags such as fluorophores and quenchers. On-demand modification of NAs may reduce the robustness of NA tests and sharply increase the test cost. In addition, the involvement of reverse transcription still remains unoptimizable for RNA detection because of the relatively high error rate.[19−21]

Received: October 13, 2020
Accepted: January 13, 2021

https://dx.doi.org/10.1021/acs.analchem.0c04303
Anal. Chem. XXXX, XXX, XXX−XXX

Herein, we report a method for profiling of SARS-CoV-2 and its mutated variants via a light-up RNA aptamer signaling-CRISPR-Cas13 amplification method. Light-up RNA aptamers are special NA affinities that could specifically bind with dyes and fix their structure to form a light-up aptamer−dye complex.[22−24] The unlabeled light-up RNA aptamer allows sensitive output of amplification signals via target-activated ribonuclease activity of CRISPR-Cas13a. Alternative to reverse transcription, a ligation strategy is introduced to initiate transcription amplification. Sequence specificity is ensured by both the ligation process and Cas13a/crRNA recognition. The feasibility for diagnosing RNA viruses was demonstrated using pseudovirus of SARS coronavirus, the Middle East respiratory syndrome (MERS) coronavirus, SARS-CoV-2, and influenza viruses. We applied the RNA assays to profile the key mutation, D614G of SARS-CoV-2 variants, and detect SARS-CoV-2 infection in throat swab, serum samples, and SARS-CoV-2 contaminations in food packaging and seafood.

EXPERIMENTAL SECTION

Materials. All DNA sequences were synthesized by Shanghai Sangon Biological Engineering Technology & Services Co., Ltd. (Shanghai, China) and purified by high performance liquid chromatography. The 5′ end of the presubstrate B was phosphorylated. Phi29 DNA polymerase (cat. no. EP0094), T7 RNA polymerase (cat. no. EP0111), NTP mixtures (cat. no. R0481), Lipofectamine 3000 (cat. no. L3000001), Random Hexamer primers (cat. no. SO142), RiboLock RNase Inhibitors (cat. no. EO0832), RevertAid RT (cat. no. K1691), and SYBR Green qPCR Supermix (cat. no. 2171875) were purchased from Thermo Fisher Scientific (Waltham, USA). T4 RNA ligase 2 (cat. no. M0239S) and dNTP mixtures (cat. no. N0447S) were provided by New England Biolabs (Beijing, China). MolPure Viral DNA/RNA Kit (cat. no. 19321ES50) was bought from Yeasen Biotech Co., Ltd. (Shanghai, China). Cas13a protein (cat. no. 32117) was bought from Tolo Biotech Co., Ltd. (Shanghai, China). DFHBI-1T dyes (cat. no. 410-1 mg) were purchased from Lucerna Technologies (NY, USA). Gelred dyes (cat. no. 41001) were bought from Biotium (Beijing, China). Total RNA extracted from influenza viruses, H1N1, H7N9, and H9N2 was kindly supplied by Prof. Yi Shi and group (CAS Key Laboratory of Pathogenic Microbiology and Immunology, Chinese Academy of Sciences, Beijing, China).

Preparation of Pseudovirus. To generate MERS, SARS, and SARS-CoV-2 pseudovirus, we applied the lentiviral vector system to produce the pseudoviruses with key genes including the N gene, E gene, and S gene (Figures S1 and S2, in the Supporting Information). The key genes including N gene, E gene, and S gene were synthesized and cloned into the PacI and NheI sites of the pCMV3 vector. The constructed recombinant plasmids were confirmed by DNA sequencing. 5×10^6 HEK293T cells were cotransfected with 6 μg of recombinant plasmids using the Lipofectamine 3000 transfection reagent. Cells were then transferred to fresh DMEM and kept for 12 h. The supernatants containing the pseudoviruses were harvested 48−72 h after transfection and filtered through a 0.45 μm filter.

Preparation of crRNA and Light-Up RNA Aptamer, Broccoli. The light-up RNA aptamer, broccoli, was chosen because of its high structure stability and fluorescence turn-on ratio.[25−27] The crRNA sequences were designed according to the reported CRISPR-Cas13a assays.[14] The mixtures containing 4 μL of DNA templates (Table S1, in the Supporting Information) of crRNA or broccoli, 4 μL of promoter sequences, 4 μL of phi29 DNA polymerase buffer, and 10.1 μL of H_2O were annealed at 90 °C for 5 min and at room temperature for 30 min. Then, 0.4 μL of phi29 DNA polymerase (10 U/μL) and 1 μL of dNTP mixtures (10 mM each for dATP, dGTP, dCTP, and dTTP) were added to the mixtures, and they were incubated at 30 °C for 30 min. After the inactivation procedure, the above mixtures were mixed with 0.5 μL of T7 RNA polymerase (20 U/μL), 8 μL of T7 RNA polymerase buffer, and 2 μL of NTP mixtures (10 mM each for ATP, GTP, CTP, and TTP) at 37 °C overnight to obtain the transcription product of crRNA and broccoli. The concentration of obtained crRNA and broccoli was quantified using a microplate reader Synergy H1 (BioTek, USA).

RNA Virus Detection. RNA genes were either extracted from pseudovirus using the MolPure Viral DNA/RNA Kit according to the manufacturer's instructions or obtained by *in-vitro* transcription. 4 μL of RNA samples, 4 μL of presubstrate A (10 μM), 4 μL of presubstrate B (10 μM), 4 μL of promoter sequences (10 μM), 1 μL of T4 RNA ligase 2 (10 U/μL), 2 μL of 10×T4 RNA ligase 2 buffer, and 8.5 μL of H_2O were mixed and incubated at 37 °C for 30 min to proceed the ligation procedure. Transcription amplification was carried out by adding 0.5 μL of T7 RNA polymerase (20 U/μL), 8 μL of T7 RNA polymerase buffer, and 2 μL of NTP mixtures (10 mM each for ATP, GTP, CTP, and TTP) at 37 °C. A volume of 40 μL was used to detect RNA viruses containing 4 μL of transcription products, 4 μL of broccoli (10 μM), 4 μL of crRNA (10 μM), 0.2 μL of LwaCas13a (10 μM), 4 μL of 10× Cas13a buffer (supplied by Tolo Biotech), 4 μL of DFHB-1T solution (100 nM), and 19.8 μL of H_2O. The mixture remained at 37 °C for 20 min for the cleavage of light-up RNA aptamer, broccoli. Next, the abovementioned mixture was prepared for fluorescence analysis.

Fluorescence Spectra and Gel Electrophoresis Analysis. Fluorescent spectra were analyzed by a microplate reader Synergy H1 (BioTek, USA). The excitation/emission wavelengths were 468/498 nm. The real-time fluorescence analysis procedure was carried out by Synergy H1, with excitation/emission wavelengths of 468/498 nm and a measurement time interval of 30 s. Nondenaturing gel electrophoresis analysis was carried out at a final reaction volume of 6 μL, containing 5 μL of oligonucleotides and 1 μL of gel loading buffer. Agarose was prepared with 50× TAE buffer and 20× Gelred dyes. Then, the gel electrophoresis was carried out at 150 V for 40 min and imaged using a Gel Doc XR+ system (Bio-Rad, USA).

Detection of SARS-CoV-2 in Throat Swab, Food Package, and Frozen Belt Fish Samples. All COVID-19 coronavirus RNA clinical samples were collected and analyzed from The West China Hospital of Sichuan University (Ethical Approval no. 2020(100)). Viral RNAs in throat swab samples were obtained by RNA extraction and virus RNA detection procedures, the same as that done in the buffer conditions. For nonclinical throat swab samples, 100, 500, and 2000 copies of SARS-CoV-2 pseudovirus were spiked in the liquid samples. For food package samples, 200 μL of solutions containing 0, 500, or 2000 copies of SARS-CoV-2 pseudovirus were spayed in a surface area of the package (with an area with a diameter of ∼3 cm) to mimic the contamination of SARS-CoV-2 virus. 300 μL of washing buffer was used to collect the SARS-CoV-2 virus on the surface of the food package. For frozen belt fish samples, fish tissues were cut and grinded by SCIENTZ-48 tissuelyser (Ningbo Scientz Biotechnology Co., Ltd, China), and then different amounts of SARS-CoV-2 pseudovirus were spiked in the samples. Total RNA was obtained from the SARS-CoV-2

https://dx.doi.org/10.1021/acs.analchem.0c04303
Anal. Chem. XXXX, XXX, XXX−XXX

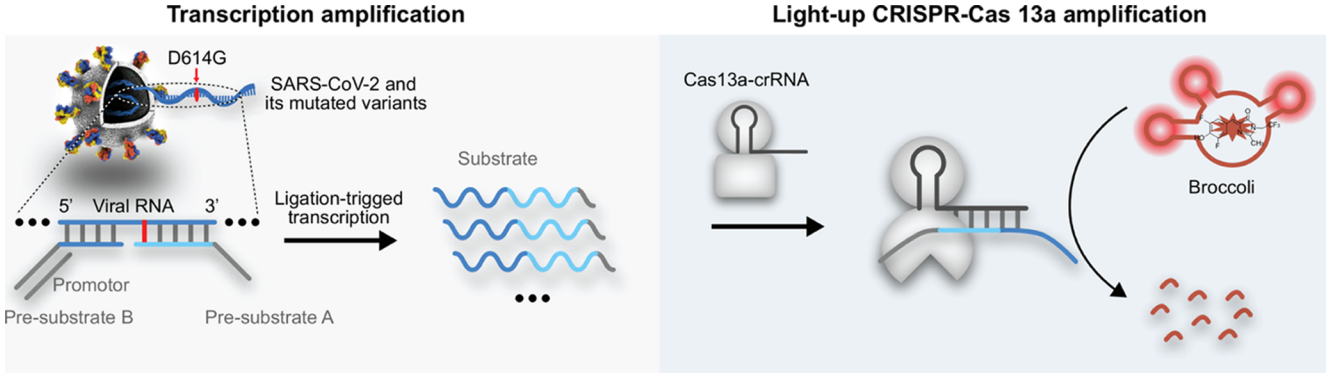

Figure 1. Schematics of the principle of detection of SARS-CoV-2 and its mutated variants via a light-up RNA aptamer signaling-CRISPR-Cas13 amplification method. Single-stranded RNA from SARS-CoV-2 serves as a template for the ligation of presubstrate probes (presubstrate A and presubstrate B), yielding a template for transcription amplification. Unlabeled light-up RNA aptamer allows sensitive output of amplification signals via the target-activated ribonuclease activity of CRISPR-Cas13a. The specificity of RNA sequences can be ensured by the ligation process and CRISPR-Cas13a recognition, thus allowing profiling of RNA viruses with a single-nucleotide resolution.

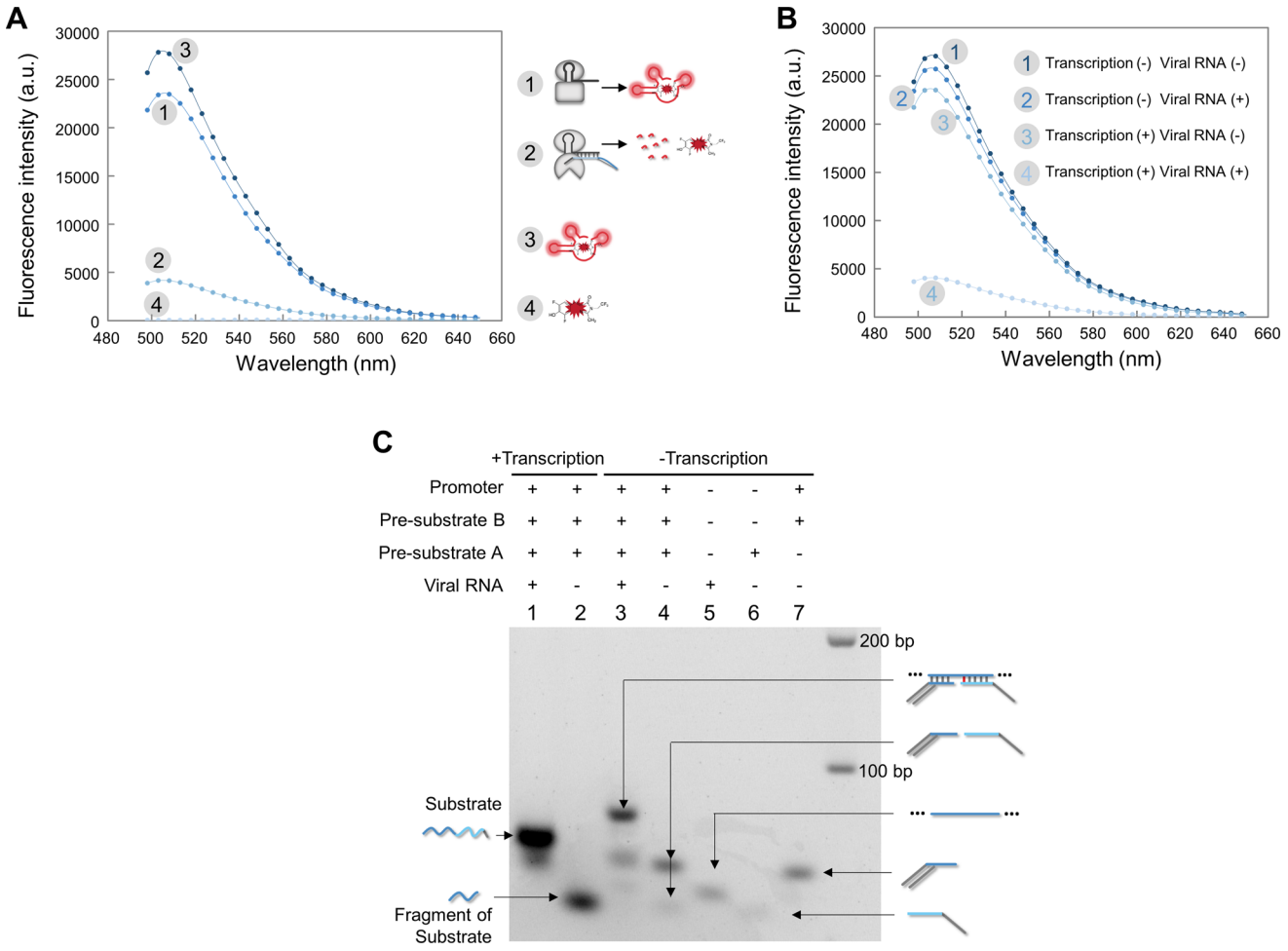

Figure 2. Investigation of the working principle of the light-up RNA aptamer signaling-CRISPR-Cas13 amplification strategy. (A) Fluorescence analysis of CRISPR-Cas13 induced cleavage of light-up RNA aptamer; (B) fluorescence analysis of RNA aptamer signaling-CRISPR-Cas13 response toward viral RNA. 5000 copies of RNA virus were added, and the concentrations of presubstrate A, presubstrate B, Cas13a, and DFHB-1T were 1 μM, 1 μM, 0.05 μM, and 10 nM, respectively, and the excitation wavelength was 468 nm. (C) Electrophoresis analysis of viral RNA-initiated transcription amplification.

virus-contaminated food package and belt fish samples using the MolPure Viral DNA/RNA Kit and analyzed by the proposed RNA assay (Figure S3, in the Supporting Information).

RT-qPCR Analysis. A 20 μL reverse transcription assay was set up containing 1 μL of Random Hexamer primer, 2 μL of RNA, 2 μL of dNTP (10 mM), 4 μL of 5× reaction buffer, 1 μL of RiboLock RNase Inhibitor (20 U/μL), 1 μL of RevertAid RT (200 U/μL), and 9 μL of H_2O. The mixture was incubated for 5 min at 25 °C followed by 60 min at 42 °C, and the reaction was terminated by heating at 70 °C for 5 min. The products were

https://dx.doi.org/10.1021/acs.analchem.0c04303
Anal. Chem. XXXX, XXX, XXX−XXX

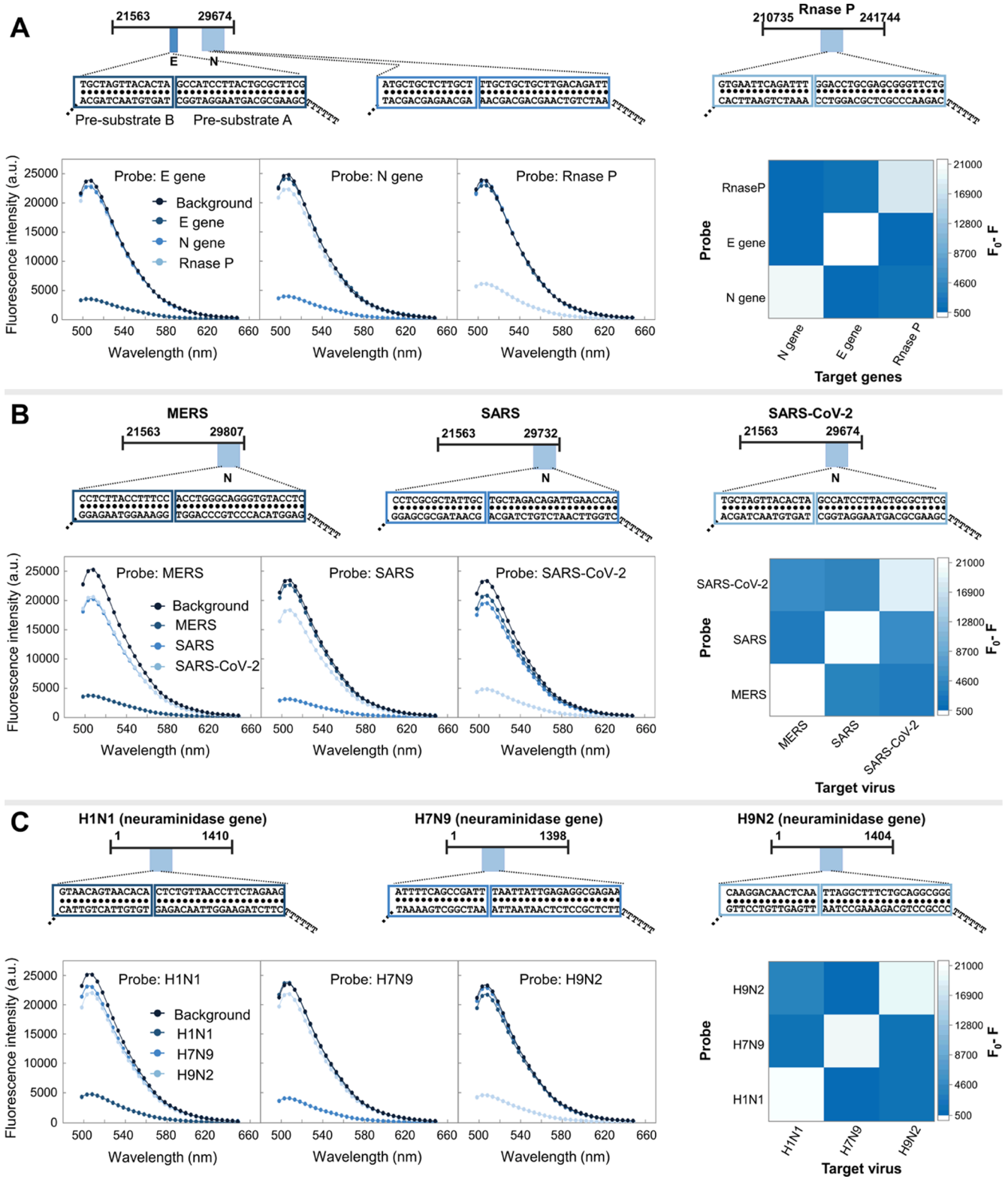

Figure 3. Profile of coronaviruses and influenza viruses. (A) Probes were designed to target N genes and E genes of SARS-CoV-2, as well as human RNase P genes; (B) detection of coronavirus species including MERS, SARS, and SARS-CoV-2; (C) detection of influenza viruses including H1N1, H7N9, and H9N2. The genome map shows the target sequences of different viruses and the sequences of Presubstrate probes. F_0 and F indicate the fluorescence intensity in the absence and presence of RNA viruses or genes, respectively. 5000 copies of RNA viruses were added, and the concentrations of presubstrate A, presubstrate B, Cas13a, and DFHB-1T were 1 μM, 1 μM, 0.05 μM, and 10 nM, respectively, and the excitation wavelength was 468 nm.

used in qPCR. A 20 μL reaction was set up containing 2 μL of products obtained in the previous step, 10 μL of SYBR Green qPCR Supermix, 2.5 μL of F-primer (4 μM), and 2.5 μL of R-primer (4 μM), followed by 95 °C for 10 min, and then 40 cycles

https://dx.doi.org/10.1021/acs.analchem.0c04303
Anal. Chem. XXXX, XXX, XXX−XXX

were carried out at 95 °C for 15 s and 60 °C for 30 s in a Bio-rad CFX96 Touch RT-PCR system (Bio-Rad, USA).

RESULTS AND DISCUSSION

Working Principles. Two processes were designed to amplify and sense the presence of RNA viruses (Figure 1). First, a split couple of probes, presubstrate A and presubstrate B, were designed to target the specific RNA sequence of SARS-CoV-2. A promoter sequence was anchored in presubstrate B. A specific ligation performed by T4 RNA ligase 2 allowed strict identification of viral RNA sequences, yielding a template for *in vitro* transcription. The ligation-based recognition process evaded reverse transcription, thus evolving a reverse transcription-free and isothermal amplification process for RNA virus detection. Next, another sequence-specific recognition process was achieved through a CRISPR RNA (crRNA) that recruited a Cas13a protein and activated its ribonuclease activity for RNA substrates. Remarkably, the introduction of light-up RNA aptamer empowered CRISPR-Cas13a for label-free detection of target RNA sequences. Dual recognition and dual amplification steps via the integration of ligation-initiated transcription amplification and CRISPR-Cas13a amplification allowed us to ensure high specificity to resolve single-nucleotide variations and high sensitivity to detect low abundant RNA viruses.

The working principle was investigated via fluorescence and electrophoresis analysis. We designed presubstrate probes targeting the N genes of SARS-CoV-2. The targeting site regions were chosen according to the published work.[12] The light-up effect of the broccoli RNA aptamer-DFHBI-1T complex was confirmed first. With the addition of RNA aptamer, broccoli, the fluorescence of DFHBI-1T was enhanced by 430 times (Figure 2A). The efficient turn-on of the RNA aptamer broccoli-DFHBI-1T complex promised a high signal-to-background ratio of RNA aptamer-signaling detection. The addition of Cas13a/crRNA induced no significant fluorescence variation. The presence of substrate sequences, however, led to a dramatic reduction of fluorescence (from 23,590 to 4183) (Figure 2A). The result indicated that substrate sequences activated the ribonuclease activity of Cas13a and substantially digested the RNA aptamer, broccoli. The substrate sequence-activated Cas13a gave an amplification effect for leveraging the response of the RNA aptamer signaling-CRISPR-Cas13 system.

We further investigated the ligation-triggered transcription amplification process. The presence of N genes dramatically reduced the fluorescence of the RNA aptamer broccoli-DFHBI-1T complex (Figure 2B), while the elimination of T7 RNA polymerase led to no significant fluorescence variation. Thus, the substantial cleavage of broccoli, RNA aptamer, resulted from the N gene-initiated transcription amplification. The process was further demonstrated by electrophoresis analysis. There emerged a lag-behind band (line 3, Figure 2C), which corresponded to an NA complex with higher molecule weight compared with the presubstrate probes. It indicated the binding of N gene sequences with both two presubstrate probes. Further addition of T7 RNA polymerase promoted the production of tremendous substrate sequences (line 1, Figure 2C). In contrast, the deletion of N gene sequences only produced the fragment of substrate sequences corresponding to presubstrate B (line 2, Figure 2C).

Profile Signatures of Coronavirus and Influenza Viruses. We then explored the ability of the RNA aptamer signaling-CRISPR-Cas13 amplification strategy for profiling coronavirus and influenza viruses. Coronaviruses are highly epidemic and pathogenic, thus posing a great threat to human health.[3] We chose three coronavirus species, MERS, SARS, and SARS-CoV-2, to estimate the feasibility of the proposed assays for RNA virus analysis. To eliminate the infection risk of these viruses, their pseudovirus counterparts were used instead. N genes, E genes, and ORF1 a/b genes of MERS, SARS, and SARS-CoV-2 were packaged in lentiviruses. The symptoms of infecting influenza virus are very similar to that of SARS-CoV-2.[4] Simultaneous profiling of the influenza virus can improve the fidelity of the SARS-CoV-2 diagnosis. Thus, probes for detecting influenza viruses (targeting neuraminidase genes) including H1N1, H7N9, and H9N2 were further designed.

First, we proposed strategies for detecting SARS-CoV-2. Current US FDA EUA guidance use both N genes and E genes to confirm the diagnosis of SARS-CoV-2.[12] Besides, the human RNase P gene is often chosen as a control to ensure the success of sampling. Thus, a probe set of presubstrate probes was designed targeting N genes, E genes of SARS-CoV-2, and RNase P gene. *In vitro*-transcribed N genes, E genes, and RNase P genes were used. The sequences of target RNA and Presubstrate probes are presented in Figure 3. The RNA aptamer signaling-CRISPR-Cas13 amplification strategy can specifically sense N genes, E genes of SARS-CoV-2, and RNase P gene (Figure 3A). Only the presence of the RNase P gene led to a slight reduction of fluorescence using probes targeting N genes. A parallel test of these three genes can imply the detection of the infection of SARS-CoV-2 with high fidelity. We then set to use the RNA aptamer signaling-CRISPR-Cas13 amplification strategy to profile different coronaviruses. N genes and E genes of three coronaviruses, MERS, SARS, and SARS-CoV-2 were chosen as target sites. We demonstrated that the RNA assay can distinguish these 3 coronavirus species, and no obvious cross-reactivity for related coronaviruses strains using probes targeting N genes and E genes (Figures 3B and S4 in the Supporting Information). The result implied the high specificity for profiling coronaviruses. In addition, RNA aptamer signaling-CRISPR-Cas13 amplification was applied for screening the influenza virus (Figure 3C). The minor cross-reactivity among influenza viruses H1N1, H7N9, and H9N2 further revealed the universality of the strategy for profiling signatures of RNA viruses. Thus, RNA aptamer signaling-CRISPR-Cas13 amplification allows the detection of different RNA viruses. Benefiting from the isothermal features of transcription amplification and homogenous reaction conditions, RNA aptamer signaling-CRISPR-Cas13 amplification promises high-throughput screening of RNA viruses using fluorescent microplate readers.

Identify Gene Mutations of SARS-CoV-2. The ability to profile the mutation of RNA viruses allows precise estimation of the epidemic and pathogenetic risk. An amino acid change in the virus' spike protein, D614G, emerged early during the pandemic, and viruses containing G614 are now dominant in many places around the world.[2] Although plenty of NA assays have been developed to diagnosis COVID19, rare tools are available to resolve gene mutations of SARS-CoV-2 virus. To estimate the ability of the assay to profile D614G mutation of SARS-CoV-2, lentiviruses containing partial S genes (wild or with D614G mutation), N genes, E genes, and ORF1 a/b genes of SARS-CoV-2 were constructed (Figure S1 in the Supporting Information). We designed a series of Presubstrate probes (1−6) to target the D614G mutation. Wild and mutated SARS-CoV-2 pseudoviruses were sequenced, and the presence of the D614G mutation was confirmed (Figure 4A). D614G mutation

https://dx.doi.org/10.1021/acs.analchem.0c04303
Anal. Chem. XXXX, XXX, XXX−XXX

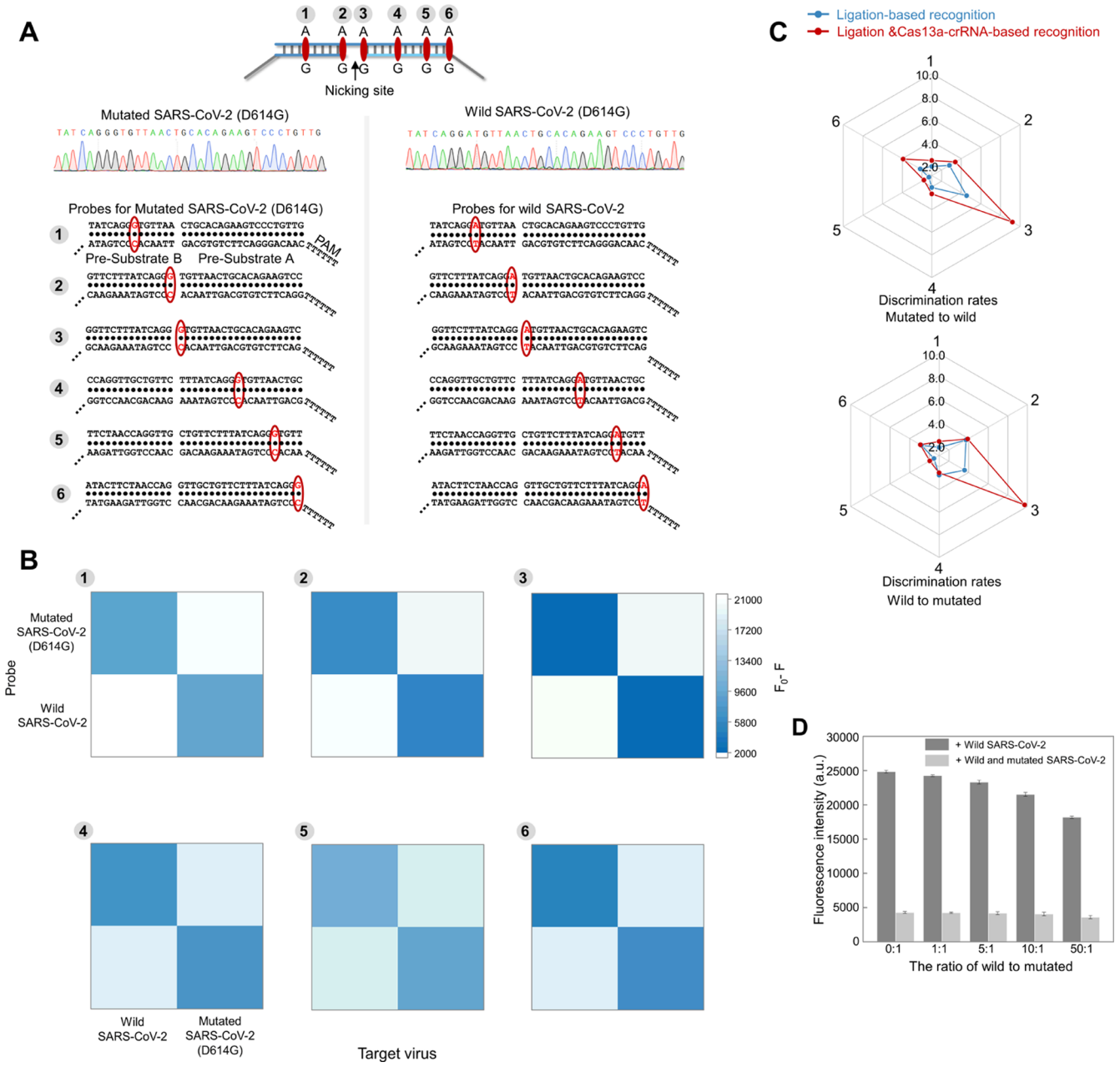

Figure 4. Identify D614G mutations of SARS-CoV-2 variants. (A) Illustration of the position of D614G mutations using a series of presubstrate probes (1-6), sequencing result of mutated and wild SARS-CoV-2, and design of presubstrate probes (1-6) for identifying D614G mutations; (B) fluorescence response ($F_0 - F$) toward mutated and wild SARS-CoV-2 using presubstrate probes 1−6. F_0 and F indicate the fluorescence intensity in the absence and presence of RNA virus, respectively; (C) discrimination rates for detecting D614G mutations using presubstrate probes 1−6; (D) fluorescence response toward wild and mutated SARS-CoV-2 virus using presubstrate probes 3. 5000 copies of RNA virus were added, and the concentrations of presubstrate A, presubstrate B, Cas13a, DFHB-1T, and SYBR Green II were 1 μM, 1 μM, 0.05 μM, 10 nM, and 1×, respectively. The excitation and emission wavelengths were 468 and 498 nm, respectively.

anchored in either presubstrate A probe or presubstrate B probe would be dramatically discriminated by the RNA assay (Figures 4B and S5, in the Supporting Information). We further defined a discrimination rate as the ratio of fluorescence response of Presubstrate probes toward its corresponding target RNA sequences (wild or mutated) to nontarget ones. We found that the position of mutation anchored close to the ligation site of presubstrate probes would yield an improved discrimination rate (such as Presubstrate probe 2 and 3). We moved the crRNA binding sites by designing crRNA with different recognition sequences. We found that the highest specificity was achieved when the mutated site was on the 5′-terminal of recognition sequences of crRNA (Figure S6, in the Supporting Information).

We further proceed to estimate the dual recognition effect on the specificity of D614G discrimination. The assays were carried out with and without Cas13a-crRNA recognition and cleavage amplification. For assays without Cas13a-crRNA recognition and cleavage amplification, the products of transcription amplification were monitored using Sybr Green II (a dye that turns on its fluorescence by binding with single-stranded RNA). The involvement of Cas13a-gRNA recognition would significantly improve the ability to discriminate the D614G mutation,

https://dx.doi.org/10.1021/acs.analchem.0c04303
Anal. Chem. XXXX, XXX, XXX−XXX

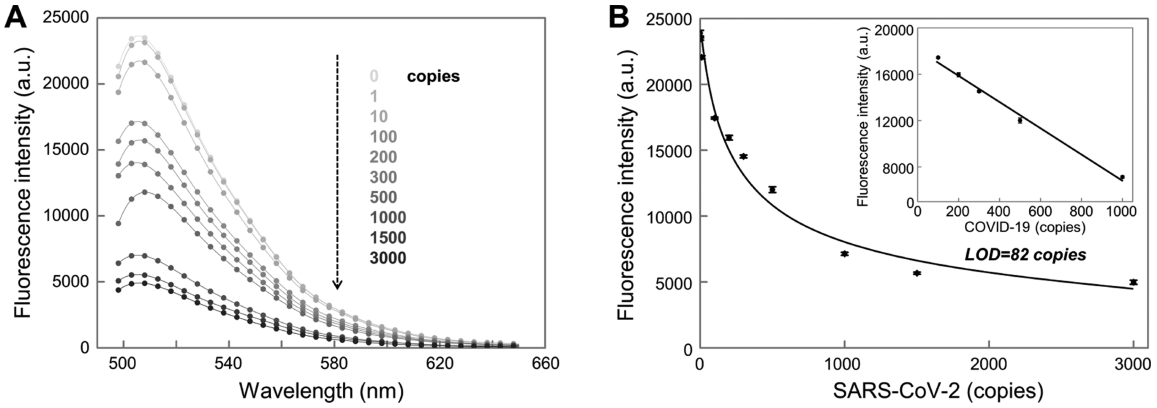

Figure 5. Quantification of SARS-CoV-2. (A) Typical fluorescence spectra of RNA aptamer signaling-CRISPR-Cas13 amplification strategy upon the addition of different copies of SARS-CoV-2 pseudovirus (0, 1, 10, 100, 200, 300, 500, 1000, 1500, and 3000 copies); (B) relationship between the copies of the SARS-CoV-2 pseudovirus and fluorescence response. (Inset) Linear relationship between the copies of the SARS-CoV-2 pseudovirus and fluorescence response. The error bars indicate the standard deviation of three parallel measurements for each concentration of SARS-CoV-2 virus. The concentrations of presubstrate A, presubstrate B, Cas13a, and DFHB-1T were 1 μM, 1 μM, 0.05 μM, and 10 nM, respectively. The excitation and emission wavelengths were 468 and 498 nm, respectively.

especially, the D614G mutation which was located on the crRNA binding sites (Figures 4C and S7, in the Supporting Information). The result further implied that the dual recognition mechanism based on the ligation process and Cas13a recognition can increase the specificity to discriminate single-nucleotide variation.

We estimated the ability of the assay to discriminate D614G mutations in the presence of wild viral RNAs. The fluorescent response of the assay toward 1, 5, 10, and 50 amounts of wild viral RNAs compared to D614G mutated viral RNAs was tested (Figure 4D). The increasing concentration of wild viral RNAs only slightly reduced the fluorescence of the assays. Even the amount of wild viral RNAs was 50 times that of D614G mutated viral RNAs, and the fluorescent variation was much smaller than that in the presence of D614G mutated viral RNAs. The results indicated that the assay can identify mutated viral RNAs even in a much higher concentration of wild viral RNAs. Thus, the presence of a dual recognition effect resulted from the ligation process and Cas13a/crRNA recognition ensured a sufficient specificity to discriminate single-nucleotide variation.

Quantification Performance. We optimized the molar ratio of Cas13a to crRNA (Figure S8, in the Supporting Information) and found that the cleavage of broccoli, RNA aptamer, can be finished within 20 min (Figure S9 in the Supporting Information). Under the optimized condition, we estimated the quantification performance of RNA aptamer signaling-CRISPR-Cas13 amplification for detecting SARS-CoV-2. Dilutions of SARS-CoV-2 pseudovirus from 0 to 3000 copies were used to determine the sensitivity of the RNA virus assay. As shown in Figure 5B, the limit of detection (LoD) for our assay was estimated to be 82 copies per reaction for the SARS-CoV-2 pseudovirus. Although, the sensitivity of the RNA virus assay was slightly lower than that of RT-qPCR.[4,6,8] The proposal of the RNA aptamer signaling-CRISPR-Cas13 amplification strategy eliminates the reverse-transcription process and chemical labeling of NA probes; further, the isothermal reaction condition further evades the dependence of expensive PCR instruments. Particularly, the RNA virus assay allows us to resolve single-nucleotide variation of SARS-CoV-2 (Table S2 in the Supporting Information). All these features promise its application for diagnosing RNA virus and viral mutations in resource-limited settings.

Detection of SARS-CoV-2 in Throat Swabs, Food Packages, and Seafoods. We utilized the RNA aptamer signaling-CRISPR-Cas13 amplification strategy for detecting SARS-CoV-2 virus from throat swabs, seafoods, and food packages. Throat swab samples are commonly used to diagnose COVID-19. SARS-CoV-2 residues in cold-chain food and food packages are highly risky for disease transmission.[28] 100, 500, and 2000 copies of SARS-CoV-2 pseudoviruses were spiked in throat swab solution samples or smeared in frozen belt fish and food packages to mimic food contaminations. For throat swab samples, the presence of 100 copies of SARS-CoV-2 pseudovirus particles led to an obvious fluorescence response compared to that of the background (Figure 6A). For food package and belt fish samples, the RNA virus detection method outputted a signal close to the background with the presence of 100 copies of SARS-CoV-2 pseudoviruses, while it induced an obvious positive response when SARS-CoV-2 pseudovirus particles were up to 500 copies. The decreased sensitivity for detecting SARS-CoV-2 in food packages and belt fish samples may be ascribed to the loss of virus during sample collection. Finally, we tested the proposed assays for analyzing clinical throat swab samples. The samples were tested by RT-qPCR and sequencing, and then analyzed by the proposed assay (Figures 6C, S10, and S11, in the Supporting Information). The proposed assay can identify throat swab samples of SARS-CoV-2 infected persons from that of healthy ones (Figure 6B, in the Supporting Information). The result preliminarily demonstrated the feasibility of the proposed assay for diagnosing COVID-19. A further test with a larger amount of COVID-19 clinical samples is needed to support its applications.

CONCLUSIONS

In this work, we have demonstrated a method for the profiling of SARS-CoV-2 and its mutated variants based on a CRISPR-Cas13 amplification principle. The CRISPR-Cas13-based amplification strategy allowed us to target and detect a series of RNA viruses including coronaviruses SARS-CoV-2, MERS, and SARS, as well as influenza viruses such as, H1N1, H7N9, and H9N2. The dual recognition processes via the ligation process and Cas13a/crRNA binding ensure a high specificity to discriminate even a single-nucleotide variation in SARS-CoV-2. Thus, the CRISPR-Cas13-based amplification strategy was

https://dx.doi.org/10.1021/acs.analchem.0c04303
Anal. Chem. XXXX, XXX, XXX−XXX

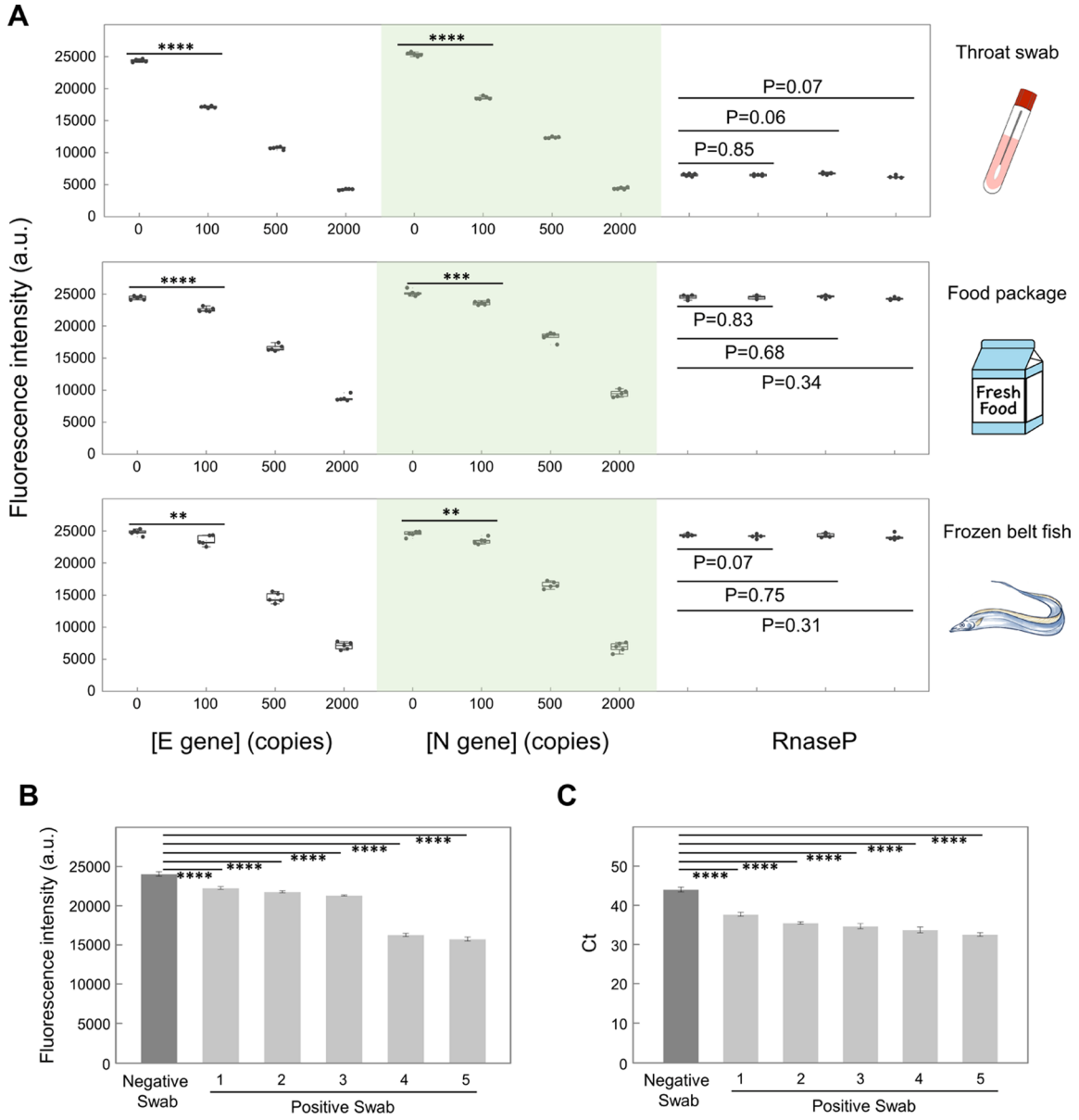

Figure 6. Detection of SARS-CoV-2 in throat swab, food packaging, frozen belt fish samples, and clinical throat swab samples. (A) SARS-CoV-2 pseudovirus particles in different copies were spiked in throat swab solutions to mimic infected samples, and spayed on surface of food packages and frozen belt fish tissues to mimic food contaminations; (B) detection of SARS-CoV-2 in clinical throat swab samples via CRISPR-Cas13-based assay; (C) detection of SARS-CoV-2 in clinical throat swab samples by RT-qPCR. The concentrations of presubstrate A, presubstrate B, Cas13a, and DFHB-1T were 1 μM, 1 μM, 0.05 μM, and 10 nM, respectively, and the excitation wavelength was 468 nm. Tests were carried in three replicates (two-tailed Student's *t*-test; $^{**}P < 0.01$, $^{***}P < 0.001$, $^{****}P < 0.0001$; bars represent ± s.d).

accommodated to profile the clinically significant mutation, D614G, of SARS-CoV-2 variants. The introduction of light-up RNA aptamers for signaling target-initiated Cas13a/crRNA ribonuclease eliminates the use of chemically labeled RNA substrates. The feasibility for profiling SARS-CoV-2 in throat swabs, seafoods, and food packages promises the use of the assays for monitoring clinical and food associated SARS-CoV-2 transmission.

■ ASSOCIATED CONTENT

Supporting Information

The Supporting Information is available free of charge at https://pubs.acs.org/doi/10.1021/acs.analchem.0c04303.

Oligonucleotide sequences; different assays for the detection of SARS-CoV-2; gene sequences of SARS-CoV-2 (wild), SARS-CoV-2 (D614G mutated), SARS and MERS pseudovirus; plasmid vector for constructing pseudovirus; working flow to prepare SARS-CoV-2 contaminated food packages and frozen belt fish samples; detection of E gene of coronavirus species; the effect of locus sites of mutation on the specificity; the effect of recognition sequences of mutation on the specificity; discrimination rates via ligation-based recognition or the integration of ligation and Cas13/crRNA recognition; optimization of the ratio of Cas13a to crRNA; real-time analysis of Cas13a-crRNA induced cleavage of light-up RNA aptamer; amplification curves of N genes of SARS-

https://dx.doi.org/10.1021/acs.analchem.0c04303
Anal. Chem. XXXX, XXX, XXX−XXX

CoV-2 from clinical throat swab samples; and sequencing of SARS-CoV-2 in clinical throat swab samples (PDF)

AUTHOR INFORMATION

Corresponding Authors

Ruijie Deng − *College of Biomass Science and Engineering, Healthy Food Evaluation Research Center, Sichuan University, Chengdu 610065, China;* orcid.org/0000-0001-9094-124X; Email: drj17@scu.edu.cn

Weimin Li − *Department of Respiratory and Critical Care Medicine, West China Medical School/West China Hospital, Sichuan University, Chengdu 610041, China;* orcid.org/0000-0003-0985-0311; Email: weimi003@scu.edu.cn

Authors

Yuxi Wang − *Department of Respiratory and Critical Care Medicine, West China Medical School/West China Hospital, Sichuan University, Chengdu 610041, China*

Yong Zhang − *College of Biomass Science and Engineering, Healthy Food Evaluation Research Center, Sichuan University, Chengdu 610065, China*

Junbo Chen − *Analytical & Testing Center, Sichuan University, Chengdu, Sichuan 610064, China*

Minjin Wang − *Department of Laboratory Medicine, West China Hospital of Sichuan University, Chengdu 610041, China*

Ting Zhang − *College of Biomass Science and Engineering, Healthy Food Evaluation Research Center, Sichuan University, Chengdu 610065, China*

Wenxin Luo − *Department of Respiratory and Critical Care Medicine, West China Medical School/West China Hospital, Sichuan University, Chengdu 610041, China*

Yalun Li − *Department of Respiratory and Critical Care Medicine, West China Medical School/West China Hospital, Sichuan University, Chengdu 610041, China*

Yangping Wu − *Department of Respiratory and Critical Care Medicine, West China Medical School/West China Hospital, Sichuan University, Chengdu 610041, China*

Bo Zeng − *Department of Respiratory and Critical Care Medicine, West China Medical School/West China Hospital, Sichuan University, Chengdu 610041, China*

Kaixiang Zhang − *School of Pharmaceutical Sciences, Key Laboratory of Targeting Therapy and Diagnosis for Critical Diseases, Zhengzhou University, Zhengzhou 450001, China;* orcid.org/0000-0002-6812-6342

Complete contact information is available at: https://pubs.acs.org/10.1021/acs.analchem.0c04303

Author Contributions

[#]Y.W. and Y.Z. contributed equally to this work.

Notes

The authors declare no competing financial interest.

ACKNOWLEDGMENTS

This work was supported by Special Funds for COVID-19 Prevention and Control of West China Hospital of Sichuan University (HX-2019-nCoV-003 and HX-2019-nCoV-042), Sichuan Science and Technology Program (2019YFS0003, 2020YFS0572, and 2020YFS0573) and Major Science and Technology Innovation Project of Chengdu City (2020-YF08-00080-GX). We are grateful to Prof. Dr. Yi Shi (CAS Key Laboratory of Pathogenic Microbiology and Immunology, Institute of Microbiology, Chinese Academy of Sciences, Beijing, China) for kindly providing the total RNA of influenza virus H1N1, H7N9, and H9N2.

REFERENCES

(1) Weber, D. J.; Rutala, W. A.; Fischer, W. A.; Kanamori, H.; Sickbert-Bennett, E. E. *Am. J. Infect. Control* **2016**, *44*, e91−e100.

(2) Korber, B.; Fischer, W. M.; Gnanakaran, S.; Yoon, H.; Theiler, J.; Abfalterer, W.; Hengartner, N.; Giorgi, E. E.; Bhattacharya, T.; Foley, B.; Hastie, K. M.; Parker, M. D.; Partridge, D. G.; Evans, C. M.; Freeman, T. M.; de Silva, T. I.; McDanal, C.; Perez, L. G.; Tang, H.; Moon-Walker, A.; et al. *Cell* **2020**, *182*, 812−827.

(3) Qin, Z.; Peng, R.; Baravik, I. K.; Liu, X. *Matter* **2020**, *3*, 628−651.

(4) Weissleder, R.; Lee, H.; Ko, J.; Pittet, M. J. *Sci. Transl. Med.* **2020**, *12*, eabc1931.

(5) Zhang, K.; Qin, S.; Wu, S.; Liang, Y.; Li, J. *Chem. Sci.* **2020**, *11*, 6352−6361.

(6) Carter, L. J.; Garner, L. V.; Smoot, J. W.; Li, Y.; Zhou, Q.; Saveson, C. J.; Sasso, J. M.; Gregg, A. C.; Soares, D. J.; Beskid, T. R.; Jervey, S. R.; Liu, C. *ACS Cent. Sci.* **2020**, *6*, 591−605.

(7) Ji, T.; Liu, Z.; Wang, G.; Guo, X.; Akbar khan, S.; Lai, C.; Chen, H.; Huang, S.; Xia, S.; Chen, B.; Jia, H.; Chen, Y.; Zhou, Q. *Biosens. Bioelectron.* **2020**, *166*, 112455.

(8) Feng, W.; Newbigging, A. M.; Le, C.; Pang, B.; Peng, H.; Cao, Y.; Wu, J.; Abbas, G.; Song, J.; Wang, D.-B.; Cui, M.; Tao, J.; Tyrrell, D. L.; Zhang, X.-E.; Zhang, H.; Le, X. C. *Anal. Chem.* **2020**, *92*, 10196−10209.

(9) Zhang, K.; Deng, R.; Gao, H.; Teng, X.; Li, J. *Chem. Soc. Rev.* **2020**, *49*, 1932−1954.

(10) Myhrvold, C.; Freije, C. A.; Gootenberg, J. S.; Abudayyeh, O. O.; Metsky, H. C.; Durbin, A. F.; Kellner, M. J.; Tan, A. L.; Paul, L. M.; Parham, L. A.; Garcia, K. F.; Barnes, K. G.; Chak, B.; Mondini, A.; Nogueira, M. L.; Isern, S.; Michael, S. F.; Lorenzana, I.; Yozwiak, N. L.; MacInnis, B. L.; et al. *Science* **2018**, *360*, 444−448.

(11) Yu, L.; Wu, S.; Hao, X.; Dong, X.; Mao, L.; Pelechano, V.; Chen, W.-H.; Yin, X. *Clin. Chem.* **2020**, *66*, 975−977.

(12) Broughton, J. P.; Deng, X.; Yu, G.; Fasching, C. L.; Servellita, V.; Singh, J.; Miao, X.; Streithorst, J. A.; Granados, A.; Sotomayor-Gonzalez, A.; Zorn, K.; Gopez, A.; Hsu, E.; Gu, W.; Miller, S.; Pan, C.-Y.; Guevara, H.; Wadford, D. A.; Chen, J. S.; Chiu, C. Y. *Nat. Biotechnol.* **2020**, *38*, 870−874.

(13) Ackerman, C. M.; Myhrvold, C.; Thakku, S. G.; Freije, C. A.; Metsky, H. C.; Yang, D. K.; Ye, S. H.; Boehm, C. K.; Kosoko-Thoroddsen, T.-S. F.; Kehe, J.; Nguyen, T. G.; Carter, A.; Kulesa, A.; Barnes, J. R.; Dugan, V. G.; Hung, D. T.; Blainey, P. C.; Sabeti, P. C. *Nature* **2020**, *582*, 277−282.

(14) Gootenberg, J. S.; Abudayyeh, O. O.; Lee, J. W.; Essletzbichler, P.; Dy, A. J.; Joung, J.; Verdine, V.; Donghia, N.; Daringer, N. M.; Freije, C. A.; Myhrvold, C.; Bhattacharyya, R. P.; Livny, J.; Regev, A.; Koonin, E. V.; Hung, D. T.; Sabeti, P. C.; Collins, J. J.; Zhang, F. *Science* **2017**, *356*, 438−442.

(15) Aman, R.; Mahas, A.; Mahfouz, M. *ACS Synth. Biol.* **2020**, *9*, 1226−1233.

(16) Gootenberg, J. S.; Abudayyeh, O. O.; Kellner, M. J.; Joung, J.; Collins, J. J.; Zhang, F. *Science* **2018**, *360*, 439−444.

(17) Kellner, M. J.; Koob, J. G.; Gootenberg, J. S.; Abudayyeh, O. O.; Zhang, F. *Nat. Protoc.* **2019**, *14*, 2986−3012.

(18) Li, Y.; Teng, X.; Zhang, K.; Deng, R.; Li, J. *Anal. Chem.* **2019**, *91*, 3989−3996.

(19) Deng, R.; Zhang, K.; Li, J. *Acc. Chem. Res.* **2017**, *50*, 1059−1068.

(20) Fungtammasan, A.; Tomaszkiewicz, M.; Campos-Sánchez, R.; Eckert, K. A.; DeGiorgio, M.; Makova, K. D. *Mol. Biol. Evol.* **2016**, *33*, 2744−2758.

(21) Ståhlberg, A.; Håkansson, J.; Xian, X.; Semb, H.; Kubista, M. *Clin. Chem.* **2004**, *50*, 509−515.

(22) Paige, J. S.; Nguyen-Duc, T.; Song, W.; Jaffrey, S. R. *Science* **2012**, *335*, 1194.

(23) Paige, J. S.; Wu, K. Y.; Jaffrey, S. R. *Science* **2011**, *333*, 642−646.

https://dx.doi.org/10.1021/acs.analchem.0c04303
Anal. Chem. XXXX, XXX, XXX−XXX

(24) Ying, Z.-M.; Wu, Z.; Tu, B.; Tan, W.; Jiang, J.-H. *J. Am. Chem. Soc.* **2017**, *139*, 9779−9782.
(25) Ying, Z.-M.; Xiao, H.-Y.; Tang, H.; Yu, R.-Q.; Jiang, J.-H. *Chem. Commun.* **2018**, *54*, 8877−8880.
(26) Neubacher, S.; Hennig, S. *Angew. Chem., Int. Ed.* **2019**, *58*, 1266−1279.
(27) Sheng, L.; Lu, Y.; Deng, S.; Liao, X.; Zhang, K.; Ding, T.; Gao, H.; Liu, D.; Deng, R.; Li, J. *Chem. Commun.* **2019**, *55*, 10096−10099.
(28) Rizou, M.; Galanakis, I. M.; Aldawoud, T. M. S.; Galanakis, C. M. *Trends Food Sci. Tech.* **2020**, *102*, 293−299.

https://dx.doi.org/10.1021/acs.analchem.0c04303
Anal. Chem. XXXX, XXX, XXX−XXX